AIP | Applied Physics Letters

Thermally activated control of microfluidic friction

Ranabir Dey, Sunando DasGupta, and Suman Chakraborty

Citation: Applied Physics Letters **101**, 134101 (2012); doi: 10.1063/1.4754605
View online: http://dx.doi.org/10.1063/1.4754605
View Table of Contents: http://scitation.aip.org/content/aip/journal/apl/101/13?ver=pdfcov
Published by the AIP Publishing

Thermally activated control of microfluidic friction

Ranabir Dey,[1] Sunando DasGupta,[2] and Suman Chakraborty[1,a)]
[1]*Department of Mechanical Engineering, Indian Institute of Technology Kharagpur, Kharagpur 721 302, West Bengal, India*
[2]*Department of Chemical Engineering, Indian Institute of Technology Kharagpur, Kharagpur 721 302, West Bengal, India*

(Received 9 May 2012; accepted 6 September 2012; published online 24 September 2012)

Contrary to the common belief that fluid friction unilaterally determines the thermal characteristics of a microfluidic device, we show here that fluid frictional characteristics of a microfluidic device may essentially be thermally tuned, delineating a non-intuitive two-way coupling. Our experiments reveal that the interfacial phenomena triggered by thermal alteration of interfaces with certain topographical and wettability characteristics may reduce the interfacial friction to a considerable extent. This has far-ranging scientific and technological consequences towards obtaining improved throughput in microfluidic devices with applications ranging from biotechnology to electronics cooling. © *2012 American Institute of Physics*. [http://dx.doi.org/10.1063/1.4754605]

Ultra-fine tunability of microfluidic structures over preferential scales has opened up newer opportunities of imposing stringent controls over frictional resistances against fluid flow. This has significant practical relevance in several miniaturized devices and systems with applications ranging from biomedical engineering and biotechnology to electronics cooling.[1,2] The underlying concepts may be judiciously employed for optimizing the energy requirements necessary towards obtaining a desired microfluidic throughput, which is a matter of immense concern to the applied research community. In general, it is believed that combinations of surface roughness/topography and wettability characteristics are likely to influence interfacial interaction, and hence microfluidic friction, in a rather profound manner.[3–19]

Although the literature on microfluidic friction is rather vast,[20,21] a common consensus that can be drawn from this literature is that surface effects bear profound influences on the flow frictional characteristics in micro and nanoscale devices. This, in turn, has been shown to influence other transport characteristics, especially the thermal transport,[22–29] in a rather prolific manner. Very recently, the dependence of atomic level stick-slip friction on the surface temperature has been explicitly delineated.[30] But such correlation has not been reported yet for experimentally resolvable fluidic scale. Hence, the nature of interfacial frictional influences has commonly been perceived to be unilateral, i.e., fluid frictional characteristics have been attributed to be responsible behind other transport characteristics but not vice versa. Contrary to this common belief percolated in the literature, here we show a mechanism by which thermally activated tunability of interfacial friction can indeed be achieved, bearing far-ranging scientific and technological consequences towards obtaining improved throughput from microfluidic devices and systems. Proceeding further, we show that a precise control towards the thermally influenced mechanism of reduction in microfluidic friction may be achieved by judiciously engineering the surface roughness and wettability characteristics.

Our experimental studies are performed with four test sections (TS-1, TS-2, TS-3, and TS-4); each consisting of a single microchannel fabricated by micromilling process on an aluminium substrate, and having identical nominal dimensions, i.e., 45 mm $(L) \times 200\,\mu$m $(W) \times 300\,\mu$m (H), as the same cutting tool and depth of cut are employed for fabricating the channels. However, these test sections, although geometrically similar, differ in their surface characteristics. In this regard, TS-1 is naturally hydrophobic, whereas the microchannel surfaces for TS-2, having comparable surface roughness magnitude as TS-1, are hydrophilized by means of plasma oxidation.[31] On the other hand, TS-3 and TS-4 have significantly different surface roughness characteristics in comparison to TS-1, as imparted by tuning the micromilling process parameters, like nature of milling process (upcut or downcut) and the feed rate during the milling procedure.[10,31] The wettability is characterized by the equilibrium contact angle (θ) of Milli-Q deionized (DI) water (Millipore Corp., Boston, MA) on respective aluminium substrates, whereas the surface roughness is characterized by the relative surface roughness ($\varepsilon = R_a/D_H$, where R_a is the average surface roughness and D_H is the microchannel hydraulic diameter) as evaluated by atomic force microscopy. The test section is integrated to an experimental setup[31] for measuring the pressure drop of DI water, flowing through the microchannel, at varying magnitudes of wall heat flux. The wall heat flux is controlled by tuning the wattage applied (by means of a DC power supply) to a couple of strip heaters, attached to the bottom of the test sections. The frictional characteristics are quantified by the Poiseuille number (Po), which is the product of the Darcy friction factor (f) and the Reynolds number (Re), and is given as $Po = f \times \mathrm{Re} = \frac{2\Delta P {D_H}^2}{L\rho(T)\nu(T)\bar{u}}$ where ΔP is the pressure drop along the microchannel as measured by a digital pressure transducer (Honeywell sensotac: 0-1 PSI), L is the axial distance between the two pressure tappings, $\rho(T)$ is the density of the DI water, $\nu(T)$ is the kinematic viscosity of water (the thermophysical properties used for determining Po are evaluated on the basis of the bulk mean temperature (T) at a definite level of heat flux and under a specific flow condition), and $\bar{u}$ is the average flow velocity. $\bar{u}$ can be

a)Author to whom correspondence should be addressed. E-mail: suman@mech.iitkgp.ernet.in.

determined from the relation, $\bar{u} = \frac{Q}{A_C}$, where Q is the flow rate of deionized water as supplied by a syringe pump (Harvard apparatus PHD 2000: 0-100 ml/min), and A_C denotes the cross-sectional area of the microchannel. In an effort to physically comprehend the effects of interfacial heat transfer on the flow frictional characteristics, as reflected by the pressure drop measurements, flow visualization experiments[31] are also conducted with the objective of studying the solid-fluid interfacial condition at the same range of applied wall heat flux. The test sections for the flow visualization have geometrical properties and surface characteristics identical to those used for the pressure-drop measurement experiments.

For the microchannels under consideration, the ratio of length to hydraulic diameter is very large ($\frac{L}{D_H} = \frac{45}{0.240} = 187.5$), and hence entrance effects can be neglected. Therefore, a laminar, hydrodynamically fully developed flow can be assumed without any loss of generality. From classical consideration, this should lead to a constant value of Po independent of Re and other parameters.[32] However, for the experiments reported herein, although Po is virtually independent of Re (corresponding to the flow rate range of 0.6–3 ml/min) at a specific supplied heat flux level,[31] the mean value (Po_{avg}) varies with alterations in the surface heating conditions. Moreover, the nature of variation of Po_{avg}, i.e., the Re-independent value, with varying wall heat flux is appreciably different for microchannels having different wettability conditions (see Fig. 1(a)), as well as for channels having different surface roughness characteristics, but same degree of wettability (see Fig. 1(b)). The supplied wall heat flux is non-dimensionalized as: $\bar{q}''_W = \frac{q''_W}{q''_{ref}} = \frac{q''_W}{(k\Delta T_{ref}/D_H)}$ where q''_W is the experimentally applied wall heat flux, k is the thermal conductivity of DI water at the bulk mean temperature, and ΔT_{ref} is the reference temperature difference for the wall heat transfer. The values of Po_{avg} for both the hydrophobic (TS-1) and hydrophilic (TS-2) channels fall below the classical limit which may be attributed to the interactions between the surface wettability and heat transfer characteristics in narrow confinements. To that end, it first needs to be appreciated that without any supplied wall heat flux, the value of Po_{avg} is much smaller for TS-1 than that for TS-2. The thermal effects on the above mentioned characteristics can be readily perceived by noting that Po_{avg} gradually decreases with increasing supplied wall heat flux for TS-1. However, for TS-2, there is no appreciable change in Po_{avg} with increasing heat flux, for the same magnitude of applied wall heat flux. Interestingly, beyond a threshold value of the heat flux, a sudden and appreciable increase in Po_{avg} can be observed for both TS-1 and TS-2.

The relatively smaller magnitude of Po_{avg} for TS-1, under unheated condition, can be attributed to the well-evidenced mechanism of apparent slip of the flowing liquid over a nanobubble layer adhering to fractions of the rough, hydrophobic surface and liquid interface.[33–37] However, the same effect is less likely to occur over a hydrophilized substrate. Hence, for TS-1, a sizeable fraction of the roughly conical-shaped submicron cavities,[31] formed at the interface by the surface roughness asperities, is covered with a less dense stable phase (nanobubbles). On the other hand, in the regions of stick flow (portions devoid of nanobubbles), these

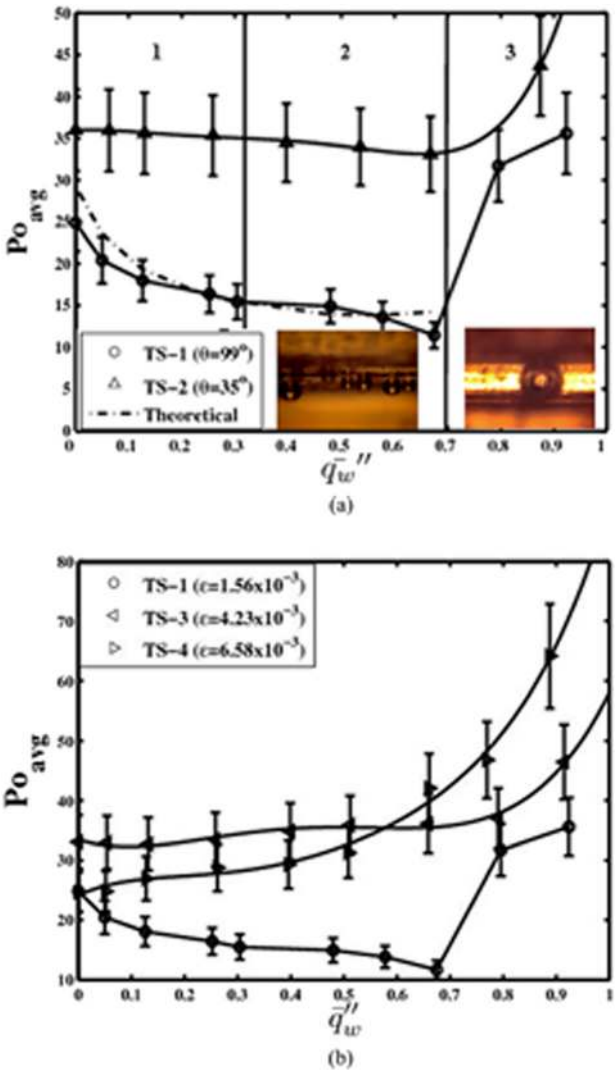

FIG. 1. Variation of flow frictional characteristics with increasing applied wall heat flux for (a) microchannels having different wettability conditions, (b) microchannels having different surface roughness characteristics. The error-bars are plotted on the basis of uncertainty analysis performed by the Kline and McClintock method.[50]

cavities are partially or totally filled by the flowing deionized water. For TS-2, the roughness cavities are generally flooded with the flowing water under unheated condition. Upon surface heating, these cavities act as localized regions of superheat resulting in evaporation of the water present in those cavities. However, the hydrophobic substrate (TS-1) has better capability of trapping the less dense phase, thus formed, than the hydrophilic substrate (TS-2), in accordance with the Bankoff's model.[38] This model proposes that only those cavities can entrap vapour or gas for which the half conical angle of the roughness cavity (β) is less than $\frac{\theta}{2}$. Hence, TS-1 contains greater density of potential vapour entrapping cavities ($\beta < 49.89°$) than TS-2 ($\beta < 17.5°$). For the latter, poor vapour entrapping capability of the surface inhomogeneities stems from the greater tendency of the flowing water to displace the entrapped vapour by flooding the cavities due to enhanced wettability of the substrate. Hence, for TS-1, as the wall heat flux is increased externally, more potential vapour entrapping cavities get superheated, thereby increasing the population density of vapour-filled cavities at the solid-fluid

interface. The less dense phase thus formed, along with the already existing nanobubble layer, results in a reduction of effective viscosity in the immediate vicinity of the wall. This subsequently decreases the bulk flow frictional behaviour for micro-confinements, culminating in the gradual decrease of Po_{avg} with increasing levels of interfacial heat flux, as delineated in regime 1 of Fig. 1(a). However, the physical paradigm of interfacial interactions gets altered altogether as the supplied heat flux level exceeds a threshold characterized by $\bar{q}''_W \sim 0.32$. For imposed heat flux levels exceeding this limit, the degree of localized superheat becomes sufficient for the vapour entrapped in the submicron cavities of TS-1 to act as nuclei for subsequent bubble growth. This leads to the formation of micron-sized bubbles at the solid-fluid interface (see Fig. 2(a)). Henceforth, as the wall heat flux is progressively increased, the nucleation site density gradually increases, thereby increasing the interfacial microbubble population (Fig. 2(b)). During the growth period of a nucleating bubble on the hydrophobic substrate, the surface tension force dominates over the buoyant force, as can be inferred from a relative order of magnitude analysis of these two effects, by taking into purview the specific wettability condition. This is represented as: $Bo = \frac{2g\Delta\rho r_b^2 f(\theta)}{3\sigma \sin^2\theta} \sim 10^{-4}$ (bond number denotes the relative importance of gravity force to surface tension force), where σ is the surface tension of the liquid, r_b is the experimentally estimated radii of the microbubbles, $\Delta\rho$ is the difference in density between the bulk liquid and the vapour phases, and $f(\theta)$ is the energy factor.[39] The dominant surface tension force facilitates the formation of roughly spherical interfacial bubbles (Fig. 2(c)) which have a reduced tendency to get detached from the channel surfaces. The gradual formation of these bubbles, with increasing heat flux, enhances the fractional coverage of the interfacial depleted density layer which aids in progressively reducing the localised viscosity near the wall. This manifests through an enhanced apparent slip, as reflected by the reduction of interfacial friction in the Po_{avg} versus $\bar{q}''_W$ characteristics, sketched in regime 2 of Fig. 1(a). However, beyond $\bar{q}''_W \sim 0.7$, the nucleating bubbles exceed a threshold size and hinder the bulk flow, ultimately leading to clogging of the micro-flow passage (Fig. 2(d)). This culminates in the sharp increase in the magnitude of Po_{avg} in regime 3 (see Fig. 1(a)). Hence, in this regime, the framework of flow friction reduction through thermally activated alteration of interfacial condition totally collapses. For TS-2, nucleation of microbubbles is found to be non-existent at smaller magnitudes of applied heat flux, which is in tune with the high energy requirement for bubble incipience on a hydrophilized substrate than on a hydrophobic substrate.[39] This, coupled with the sparse bubble population density, due to its poor vapour entrapping capability, fails to cause any appreciable reduction in interfacial friction, for imposed heat flux even below the critical threshold ($\bar{q}''_W < 0.7$), as compared to TS-1. Although, with further increase in the heat flux the bubble population increases, but the sizes of the bubbles also increase in tandem, and exceed a critical limit; thereby resulting in bulk flow hindrance, and hence a sudden increase in Po_{avg}. It is pertinent to mention here that the formation of a less dense phase in the vicinity of a solid wall, mainly through near-wall boiling or injection of microbubbles, is classically utilized for drag reduction in high Reynolds number macroscale flows/external flows, especially for

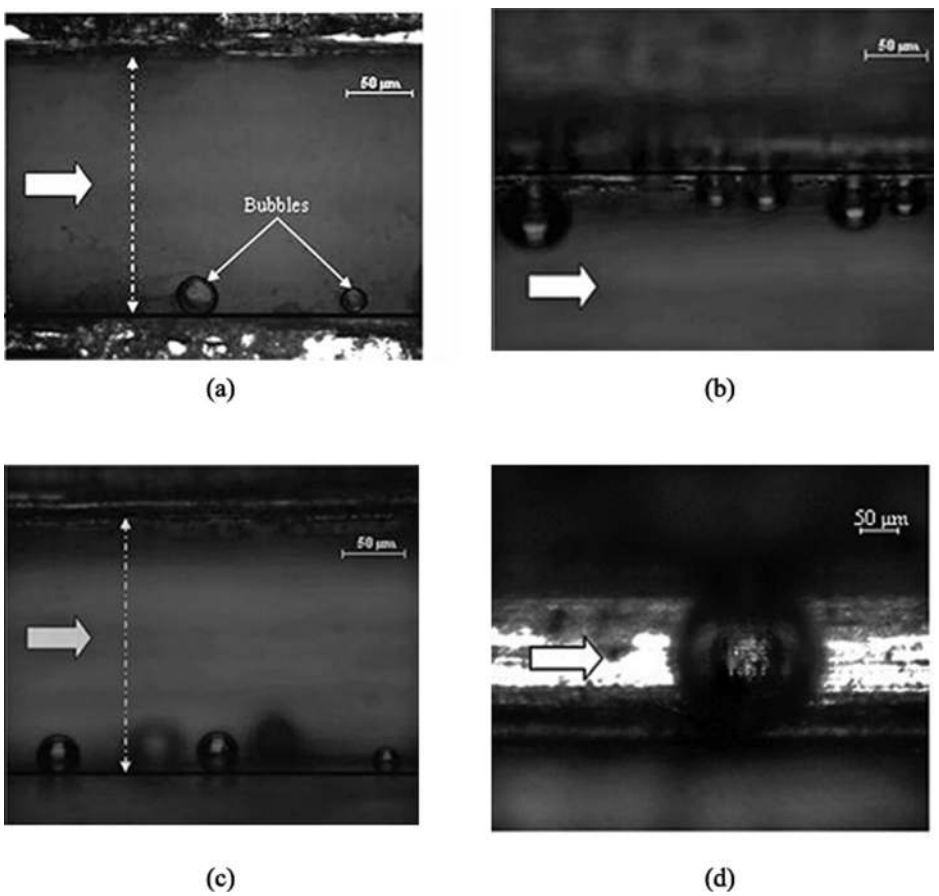

FIG. 2. (a) Nucleation of microbubbles at the solid-liquid interface on TS-1 for the non-dimensional heat flux value of 0.32. (b) Increased number density of interfacial microbubbles at a higher heat flux of 0.46. (c) Interfacial bubbles attain a spherical shape with definite radii. (d) Nucleating bubbles tending to obstruct the flow passage in TS-1 for higher heat flux levels beyond 0.7.

enhancing the performances of underwater vehicles/missiles and ships.[40–47] However, thermally controlled reduction in low Reynolds number flow friction at the microscale, as detailed herein, has never been reported previously.

The minimum degree of superheat necessary for the nucleation of stable bubbles from the nanometer-scale roughness cavities, on the microchannel substrate, is specified by fundamental thermodynamic considerations as:[38] $\Delta T_g \approx \frac{2\sigma T_{sat}}{h_{fg}\rho_g r_c}$, where r_c is the roughness cavity mouth radius, T_{sat} is the saturation temperature of the liquid, h_{fg} is the enthalpy of vapourization, ρ_g is the density of the vapour, and $\Delta T_g = (T_g - T_{sat})$ is the degree of superheat of the entrapped vapour, which is dependent on the magnitude of imposed wall heat flux. In accordance with this, for TS-3 and TS-4, which have greater surface roughness (and hence greater r_c) than TS-1, the interfacial bubble incipience starts from progressively lower levels of superheat corresponding to smaller magnitudes of wall heat flux ($\bar{q}''_W < 0.32$). However, the nucleating bubbles grow to relatively larger sizes, under identical wall heating and flow conditions, with increasing surface roughness (Fig. 3). The relatively larger sizes of the microbubbles may be attributed to the greater degree of bubble coalescence, during initial stages of their growth, due to the greater density of active nucleation sites on the rougher substrates. These relatively larger bubbles offer hindrance to the bulk flow. Therefore, a threshold value for the interfacial microbubble radius can now be defined ($r_b/D_H \approx 0.13$: evaluated from the analysis of microbubble sizes for TS-1), which, when exceeded, does not lead to the reduction of flow friction through the mechanism of apparent slip of the flowing liquid, but tends to augment the flow resistance. Hence for TS-3, the flow frictional characteristics gradually increase with externally controlled alteration of the wall heating condition due to the interfacial resistance imparted by the nucleating bubbles even at lower levels of heat flux. Beyond $\bar{q}''_W \sim 0.7$, the bubbles actually clog the flow passage culminating in a steeper increase of Po_{avg}. For TS-4, nucleating microbubbles impart relatively greater interfacial resistance at a particular heat flux level, as compared to TS-3, due to their even larger sizes and greater population density. This results in a faster rate of enhancement of interfacial friction with variation in $\bar{q}''_W$, which culminates in the steeper monotonic increase of Po_{avg} for the entire heat flux range (see Fig. 1(b)).

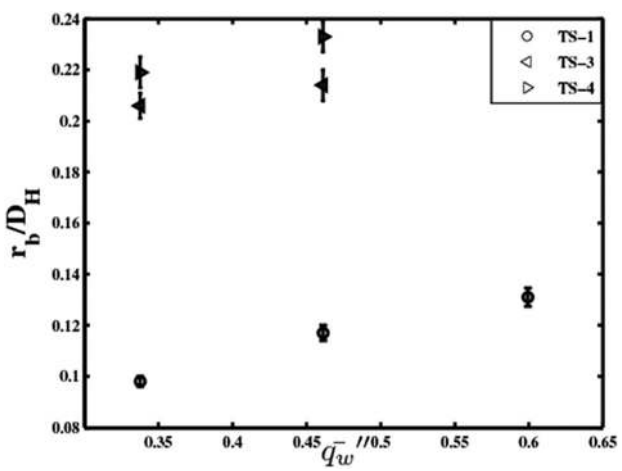

FIG. 3. Variation of average non-dimensional microbubble radius with supplied wall heat flux for three different substrates having increasing surface roughness magnitudes. The bubble-radii are evaluated by post processing the flow visualization images using IMAGE-PRO EXPRESS 6.0 software.

Here, an attempt is also made to delineate a theoretical framework that addresses the thermally controlled reduction of interfacial friction for pressure-driven microflows over substrates having optimum wettability and roughness conditions. The thermally induced reduction in frictional characteristics, over the range of heat flux implemented in this study, originates out of the interplay of the formation of an interfacial depleted density layer, and the consequential reduction in the localized viscosity of the flowing liquid. The hydrodynamics of the bulk liquid flow over the interfacial less viscous phase is modelled considering low Reynolds number pressure-driven flow of two immiscible fluids between two infinite parallel plates.[48] For the stick flow regime, i.e., the region devoid of any intervening layer, frictional characteristic is modelled by approximating the exposed rough surface as a superposition of spatial waves of increasing frequencies. The properties of the random surface roughness are then described by the pertinent correlation function, taken to be of the Gaussian form for the present study. The effective stick-slip length, for this regime, is evaluated by implementing the power spectrum density method which involves the determination of the Fourier image of the Gaussian correlation function.[10,49] The overall friction factor is expressed as a weighted average of these two effects and can be written as

$$Po_{th} = \left[\frac{32}{\gamma}A + \frac{4(1-A)}{C - D\frac{4}{\sqrt{\pi}}\left(\frac{R_a}{D_H}\right)^2\left(\frac{D_H}{l}\right)}\right] \times f_{H-K}, \quad (1)$$

where A is the weighting function, physically representing the fraction of the interface covered by the thermally tunable depleted density layer, C and D are numerical fitting parameters, l is the roughness correlation length, $f_{H\text{-}K}$ is the Hartnett-Kostic polynomial correction factor, which takes into consideration the non-infinite extent of the rectangular channel,[10] and $\gamma = \frac{1}{3} + \Omega(T)\left[4\frac{\delta(\bar{q}''_W)}{D_H} + 8\left(\frac{\delta(\bar{q}''_W)}{D_H}\right)^2\right]$. Here, $\Omega(T)$ is a function representing the ratio of the temperature-dependent viscosity of the bulk liquid to that of the depleted density layer, and $\delta(\bar{q}''_W)$ is the thickness of this intervening layer; both these functions are strongly dependent on the level of applied heat flux. Because of a linearly varying axial profile of the bulk mean temperature under constant wall heat flux, the average of the inlet and the outlet bulk mean temperature may be taken as a basis for evaluating the function $\Omega(T)$. The nature of the correlation between $\delta(\bar{q}''_W)$ and $\bar{q}''_W$ is approximated empirically, by appropriate fitting of the experimentally evaluated variation of the microbubble sizes with supplied heat flux. Although such fitting relation is more appropriate for regime 2 (Fig. 1(a)), it is extended to take into purview the interfacial phenomenon in regime 1, as it is impossible to experimentally evaluate the extent of the layer formed by the vapour-entrapped cavities which is well

beyond the resolution of the involved microscopy technique. It is important to note here that the thermally induced variation in liquid viscosity with varying wall heat flux, as aptly captured by $\Omega(T)$ in the proposed model through its dependence on the temperature-dependent liquid viscosity distribution, is intrinsic to the underlying physics dictating the thermally controlled reduction of microscale flow friction. This is substantiated by the fact that on excluding the reduction in liquid viscosity with increasing temperature corresponding to increasing wall heat flux, i.e., on considering solely the effects of formation of an interfacial layer of less dense phase with thermally alterable thickness, the model underestimates the total decrease in flow friction (44.15%) over the imposed wall heat flux range, as compared to the experimentally observed friction reduction (54.02%). This stems from the fact that preclusion of the appropriate reduced liquid viscosity from the model leads to appreciable overestimation of the Poiseuille number at a definite level of wall heat flux. Hence, it is only on considering the cumulative effects of pertinent temperature-dependent liquid viscosity variation and the formation of an intervening depleted density layer, the above proposed theoretical framework shows good coherence with the experimental data (see Fig. 1(a)), and can be considered to fairly predict the reduction in flow frictional characteristics with increasing heat flux, by taking into consideration the specific surface characteristics of the flow conduit.

In conclusion, it can be summarized that flow frictional characteristics for pressure-driven microflows can be controlled thermally. The imposed thermal effects alter the interfacial interaction in the vicinity of the channel walls; the nature of which is intrinsically dependent on the magnitude of heat flux and surface characteristics of the channels. For an optimum wettability and roughness condition, the supplied heat flux influences the interfacial condition in a manner which leads to progressive reduction of frictional characteristics. This may be judiciously utilized in designing "smart" microscale cooling techniques.

The authors would like to acknowledge the financial support provided by the Department of Information and Technology (Administrative Approval Nos. 9(2)/2006-mdd and 23/3/2007), Government of India, for this research. They would also like to thank Mr. Arup Kar for his assistance in fabricating the microchannels used in this work.

[1]T. M. Squires and S. R. Quake, Rev. Mod. Phys. **77**, 977 (2005).
[2]V. Singhal, S. V. Garimella, and A. Raman, Appl. Mech. Rev. **57**, 191 (2004).
[3]X. Gu and M. Chen, Appl. Phys. Lett. **99**, 063101 (2011).
[4]Y. P. Cheng, C. J. Teo, and B. C. Khoo, Phys. Fluids **21**, 122004 (2009).
[5]P. Tsai, A. M. Peters, C. Pirat, M. Wessling, R. G. H. Lammertink, and D. Lohse, Phys. Fluids **21**, 112002 (2009).
[6]G. M. Mala and D. Li, Int. J. Heat Fluid Flow **20**, 142 (1999).
[7]C. Kleinstreuer and J. Koo, J. Fluids Eng. **126**, 1 (2004).
[8]P. G. de Gennes, Langmuir **18**, 3413 (2002).
[9]S. Chakraborty, Appl. Phys. Lett. **90**, 034108 (2007).
[10]S. Chakraborty, T. Das, and S. Chattoraj, J. Appl. Phys. **102**, 104907 (2007).
[11]C.-H. Choi, U. Ulmanella, J. Kim, C.-M. Ho, and C.-J. Kim, Phys. Fluids **18**, 087105 (2006).
[12]C. Cottin-Bizonne, J.-L. Barrat, L. Bocquet, and E. Charlain, Nature Mater. **2**, 238 (2003).
[13]S. C. Yang, Microfluid. Nanofluid. **2**, 501 (2006).
[14]J. Ou, B. Puot, and J. P. Rothstein, Phys. Fluids **16**, 4635 (2004).
[15]C. Kunert and J. Harting, Int. J. Comput. Fluid Dyn. **22**(7), 475 (2008).
[16]D. Bryan, J. Kim, H. S. Ko, and H. C. Park, Phys. Fluids **20**, 113601 (2008).
[17]P. Tabeling, Lab Chip **9**, 2428 (2009).
[18]P. Ligrani, D. Blanchard, and B. Gale, Phys. Fluids **22**, 052002 (2010).
[19]T. Yamada, C. Hong, O. J. Gregory, and M. Faghri, Microfluid. Nanofluid. **11**, 45 (2011).
[20]G. Morini, Int. J. Therm. Sci. **43**, 631 (2004).
[21]R. Dey, T. Das, and S. Chakraborty, Heat Transfer Eng. **33**(4–5), 425 (2012).
[22]O. Shishkina and C. Wagner, J. Fluid Mech. **686**, 568 (2011).
[23]M.-N. Sabry, IEEE Trans. Compon., Packag. Technol. **23**(3), 562 (2000).
[24]W. Qu and I. Mudawar, Int. J. Heat Mass Transfer **45**, 2549 (2002).
[25]G. Rosengarten, J. Cooperwhite, and G. Metcalfe, Int. J. Heat Mass Transfer **49**, 4161 (2006).
[26]W. Qu, G. M. Mala, and D. Li, Int. J. Heat Mass Transfer **43**, 3925 (2000).
[27]S. Shen, J. L. Xu, J. J. Zhou, and Y Chen, Energy Convers. Manage. **47**, 1311 (2006).
[28]H. Y. Wu and P. Cheng, Int. J. Heat Mass Transfer **46**, 2547 (2003).
[29]S. S. Hsieh and C. Y. Lin, Int. J. Heat Mass Transfer **52**, 260 (2009).
[30]L. Jansen, H. Holscher, H. Fuchs, and A. Schirmeisen, Phys. Rev. Lett. **104**, 256101 (2010).
[31]See supplementary material at http://dx.doi.org/10.1063/1.4754605 for details of the test sections, integrated setups, and experimental conditions.
[32]F. M. White, *Viscous Fluid Flow*, 3rd ed. (McGraw-Hill, 2006).
[33]B. Borkent, S. Dammer, H. Schönherr, G. Vancso, and D. Lohse, Phys. Rev. Lett. **98**, 204502 (2007).
[34]J. Tyrrell and P. Attard, Phys. Rev. Lett. **87**, 176104 (2001).
[35]X. H. Zhang, N. Maeda, and V. S. J. Craig, Langmuir **22**, 5025 (2006).
[36]S. Yang, S. M. Dammer, N. Bremond, H. J. W. Zandvliet, E. S. Kooij, and D. Lohse, Langmuir **23**, 7072 (2007).
[37]M. Brenner and D. Lohse, Phys. Rev. Lett. **101**, 214505 (2008).
[38]C. H. Wang and V. K. Dhir, ASME J. Heat Transfer **115**, 670 (1993).
[39]H. T. Phan, N. Caney, P. Marty, S. Colasson, and J. Gavillet, Int. J. Heat Mass Transfer **52**, 5459 (2009).
[40]Y. A. Hassan and C. C. Gutierrez-Torres, Nucl. Eng. Technol. **38**, 763 (2006).
[41]W. C. Sanders, E. S. Winkel, D. R. Dowling, M. Perlin, and S. L. Ceccio, J. Fluid Mech. **552**, 353 (2006).
[42]X. Shen, S. L. Ceccio, and M. Perlin, Exp. Fluids **41**, 415 (2006).
[43]H. Kato, K. Miura, H. Yamaguchi, and M. Miyanga, J. Mar. Sci. Technol. **3**, 122 (1998).
[44]S. L. Ceccio, Annu. Rev. Fluid Mech. **42**, 183 (2010).
[45]C. Lee and C.-J. Kim, Phys. Rev. Lett. **106**, 014502 (2011).
[46]I. U. Vakerleski, J. O. Marston, D. Y. C. Chan, and S. T. Thoroddsen, Phys. Rev. Lett. **106**, 214501 (2011).
[47]M. Xiang, S. C. P. Cheung, J. Y. Tu, and W. H. Zhang, Ocean Eng. **38**, 2023 (2011).
[48]D. C. Tretheway and C. D. Meinhart, Phys. Fluids **16**, 1509 (2004).
[49]I. Ponomarev and A. Meyerovich, Phys. Rev. E **67**, 026302 (2003).
[50]J. P. Holman, *Experimental Methods for Engineers*, 7th ed. (Tata McGraw-Hill, New Delhi, 2007).